Electromagnetic Radiation from Ingested Sources in the Human Intestine between 150 MHz and 1.2 GHz

Lawrence C. Chirwa*, Paul A. Hammond, *Student Member, IEEE*, Scott Roy, and David R. S. Cumming, *Member, IEEE*

***Abstract*—The conventional method of diagnosing disorders of the human gastro-intestinal (GI) tract is by sensors embedded in cannulae that are inserted through the anus, mouth, or nose. However, these cannulae cause significant patient discomfort and cannot be used in the small intestine. As a result, there is considerable ongoing work in developing wireless sensors that can be used in the small intestine. The radiation characteristics of sources in the GI tract cannot be readily calculated due to the complexity of the human body and its composite tissues, each with different electrical characteristics. In addition, the compact antennas used are electrically small, making them inefficient radiators. This paper presents radiation characteristics for sources in the GI tract that should allow for the optimum design of more efficient telemetry systems. The characteristics are determined using the finite-difference time-domain method with a realistic antenna model on an established fully segmented human body model. Radiation intensity outside the body was found to have a Gaussian-form relationship with frequency. Maximum radiation occurs between 450 and 900 MHz. The gut region was found generally to inhibit vertically polarized electric fields more than horizontally polarized fields.**

***Index Terms*—Bio-telemetry, electromagnetic, finite-difference time-domain—FDTD, gastro-intestinal tract, human body, radiation characteristics, sensor.**

I. Introduction

THE internal monitoring and examination of the human digestive tract has conventionally been by means of sensors embedded in flexible cannulae. For diagnosis of ailments in the oesophagus, stomach, and duodenum, the cannula is inserted through the mouth or nose, while for the colon it is inserted through the anus. The cannula is attached either to a portable recorder that may be carried at the waist or a larger nonportable recording and analysis device. These current measuring methods are often unpleasant for the patient. Where cannula is inserted through the mouth or nose the throat is usually sprayed with a local anaesthetic to help prevent gagging and in all cases analgesic or sedative may be required to help the patient relax during the examination. In addition, the use of such cannulae is limited to the oesophagus, stomach, duodenum, and colon.

As a result, there are considerable ongoing efforts in developing small wireless devices that can be swallowed for examination of the whole alimentary canal. Sensors, their associated circuitry, and a transmitter are encased in "capsules" that are small enough to be swallowed and traverse the entire digestive tract while transmitting readings to an external receiver. There is no physical link between the sensors and the recording device that may either be portable, and carried by the patient, or not. Such wireless capsule methods avoid patient discomfort and need for additional medication, circumvent complications due to lining puncture that exist with the current methods, and importantly, allow examination of a region of the small intestine that is presently impossible using cannulae. They will also allow patients to go about normal life while being examined.

Remote telemetry devices have previously been used to measure ECG, EEG, temperature, pH, pressure, chemical analyte concentrations, and heart rate among other parameters [1]–[7] for both human and animal subjects. However, there has been very little work considering the use of telemetry devices in the small intestine. Such studies will contribute to advances in diagnosis, treatment, and a better understanding of the function and related ailments of the digestive tract. These devices may in the long term become routine gastro-intestinal (GI) diagnostic tools.

There has been considerable study of the effects of the human body on the radiated fields of various electromagnetic radiators [8]–[16]. All but one of these studies has been on electromagnetic fields from external sources. Until recently, investigations of implanted sources have not used realistic human body models. The first implanted source work to use such a model is that of [11], where the radio wave propagation characteristics of a source implanted in the vagina were investigated. However, the models used were semi-segmented for a region up to 300 mm from the source, while the rest of the models were tissue layered. In this paper, a realistic fully segmented body model is used in conjunction with a realistic model for a helical antenna.

The electrical properties of human tissue, namely conductivity and permittivity, are frequency dependent in such a manner that the absorption of electromagnetic waves by human tissue increases with increasing frequency. Thus, reflection at boundaries, scattering, absorption, and refraction of electromagnetic fields are frequency dependent. However, the radiation from electrically small sources in free-space increases with frequency and, in addition, the effect of the capacitive loading of the surrounding tissue on the source has an as yet unknown frequency and spatial dependence. It is apparent that the radiation characteristics of implanted sources cannot be readily estimated due to the complexity of the human body and its composite tissues, each with different electrical characteristics. Furthermore, efficient telemetry

Manuscript received November 30, 2002; revised November 5, 2002. *Asterisk indicates corresponding author.*

*L. C. Chirwa is with the Micro Systems Technology Group, Department of Electronics and Electrical Engineering, Glasgow University, Rankine Bldg., Oakfield Avenue, Glasgow G12 8LT, U.K. (e-mail: d.cumming@elec.gla.ac.uk).

P. A. Hammond, S. Roy, and D. R. S. Cumming are with the Micro Systems Technology Group, Department of Electronics and Electrical Engineering, Glasgow University, Glasgow G12 8LT, U.K.

Digital Object Identifier 10.1109/TBME.2003.809474

systems will be required in view of these devices being battery operated, especially since the compact antennas used are electrically small, making them inherently inefficient radiators. Indeed commercial transmitting models yield about 0.005% dc to radiation power conversion efficiency [11] assuming no transmitter circuit—antenna impedance mismatch. An accurate estimate of radiation characteristics is important in wireless telemetry systems especially in this case where the radiation efficiency and source power are very low and the radiation characteristics not readily predictable. This paper determines the radiation characteristics of electromagnetic sources in the GI tract, using the finite-difference time-domain (FDTD) method. It has a direct bearing on the development of wireless telemetry systems for the human intestine by providing insight into electromagnetic radiated field characteristics allowing for the optimization of designs for more power efficient telemetry systems.

The numerical modeling, human body model and the type of radiating source employed in this paper are described in Section II. Near-field results are presented in Section III and far-field results in Section IV.

II. Modelling and Analysis

A. Computational Method

The FDTD method used is based on the calculation of Maxwell's differential electromagnetic field equations. It is a versatile technique appropriate for evaluating electromagnetic fields in complex structures. In addition, its relatively simple formulation makes it efficient to implement. It is, therefore, the most popular choice for human body related electromagnetic simulation. It has been proven to yield reliably credible results in numerous cases where it has been used with human body models.

The normal use of FDTD applies a wide-band excitation to the system, allowing characteristics to be determined with good resolution (determined by the order of the discrete Fourier transform used) as a function of frequency over the whole excitation bandwidth in a single simulation run. This method, though efficient, was not used here due to the nature of the source model. The model used requires specific phase and magnitude relationships between its composite source elements, therefore, simulations had to be performed for each specific frequency. Simulations were carried out for 150, 300, 434, 600, and 800 MHz and 1.0 and 1.2 GHz. These frequencies fall in and around the range recommended as pan-European frequency allocations for short-range applications,[1] and the US Federal Communications Commission (FCC) frequency allocations for bio-medical telemetry and industrial, scientific and medical devices (regulations S5.150, US209, and US350).

The electromagnetic excitations used were of a ramped-sinusoidal form with the ramp reaching its maximum after 173 time steps. The number of time steps used ranged from 30 000 for 150-MHz sources to 20 000 for 1.2-GHz sources. In each case, these were the number of time steps required to ensure that a steady state had been achieved. Liao's absorbing boundary conditions (ABCs) [18] were used rather than perfectly matched layer (PML) ABCs [19]. When PML ABCs are used a slightly smaller FDTD work space is required than when Liao ABCs are used. However, Liao ABC terminated workspaces take considerably less time to compute than those of equal size terminated by PML ABCs, for approximately the same level of accuracy. PML solutions take about 40% longer than Liao solutions (if no magnetic materials are present) for the same size of workspace.

[1]REMCOM Inc., State College, PA

B. Human Body Model

The FDTD mesh of a male human subject used was supplied by REMCOM Inc. It was created using digitized data in the form of transverse color images from the Visible Human Project sponsored by the USA National Library of Medicine [20]. It was generated using axial anatomical images since these had the finest resolution for the entire body in the Visible Human Project. In the project, the axial anatomical cross sections are at 1-mm intervals. They are 2048 pixels by 1216 pixels. The generated model is made up of cubic voxels with an edge size of 5 mm. This cell size takes into consideration the computer resources that would be required for FDTD simulation on a relatively fast computer (in this case about 150 MB of memory for the mesh and about 6 h run time on a machine with a 1.5-GHz Pentium-IV processor). The entire human body mesh, including a minimum 20 free-space cell buffer between the body and the outer boundary of the FDTD workspace, is $136 \times 87 \times 397$ or 4 697 304 cells. Each voxel edge in the mesh is defined as one of 25 groups of tissue types. Six of these groups contain more than one tissue type with similar properties. For each tissue group, the respective material density, conductivity, and relative permittivity were assigned for all frequencies. The values of properties of human body tissue used in this investigation are shown in Table I.

C. Source Model

Practical capsule devices have been documented in [25]–[28]. The capsule casings and circuitry have been found to have negligible effect on the resident antenna's radiation, as a result there was no need to take the effects of the casing into account in the modeling of the antenna. A typical capsule device may allow an antenna with dimensions of approximately $4 \times 8 \times 8$ mm. Clearly, the relatively large grid size of 5 mm used here does not allow for the modeling of an antenna of such dimensions in adequate detail to obtain credible results [22]. In addition, a one-cell (delta gap) [21] excitation is employed where the excitation feed gap corresponds to one entire spatial interval of the FDTD lattice. However, in this case the size of the feeding gap is comparable with that of the antenna being modeled, which results in errors in FDTD calculation results. As a result, the model of a normal mode monofilar helix antenna similar to that in [10] was employed. The model is relatively simple to implement. It uses a series of equivalent electric and magnetic sources to produce the fields of a monofilar helix operating in the normal mode, where the electric and magnetic fields are related by

$$\frac{E}{H} = \frac{2S}{j\omega\epsilon_o \pi D\delta} \tag{1}$$

where E and H are the magnitudes of the electric and magnetic fields, respectively; S is the pitch and D the diameter of the

TABLE I
PROPERTIES OF HUMAN BODY TISSUE

Tissue	Property	150 MHz	300 MHz	434 MHz	600 MHz	800 MHz	1 GHz	1.2 GHz
skin	σ	0.487308	0.534727	0.56975	0.609739	0.672518	0.710805	0.763077
	ϵ	51.05	43.7502	41.6305	40.429	39.7204	39.5546	39.67
tendon, pancreas	σ	0.622081	0.7008	0.755585	0.822324	0.908543	0.970662	1.02163
prostate, aorta	ϵ	59.6815	52.99	50.5306	48.8169	47.401	46.325	46.6515
fat	σ	0.035	0.041784	0.0450363	0.0503992	0.052	0.054069	0.056065
yellow marrow	ϵ	5.78956	5.2181	5.02745	4.90799	4.84427	4.72728	4.57747
cortical bone	σ	0.0785038	0.0962836	0.111449	0.128895	0.16024	0.185962	0.211879
	ϵ	15.6001	14.09	13.4801	13.0366	12.7548	12.4722	12.3982
cancellous bone	σ	0.169947	0.20557	0.227522	0.25791	0.292778	0.326698	0.359371
	ϵ	26.1674	22.227	21.0783	20.3238	18.8216	18.436	18.3099
blood	σ	1.644	1.69	1.71976	1.77177	1.83107	1.90981	1.98462
	ϵ	65.2	58.3968	57.3049	56.4645	55.6929	55.3509	54.9846
colon, heart, spleen,	σ	0.840948	0.92413	0.985619	1.06095	1.15759	1.28749	1.43579
muscle, tongue	ϵ	74.1661	66.268	63.673	61.87593	60.7494	59.9675	59.4195
grey matter	σ	0.726775	0.82535	0.877568	0.93806	1.0093	1.12315	1.23148
cerebellum	ϵ	72.4371	58.305	54.2647	51.9561	50.6122	49.9416	50.2558
white matter	σ	0.408927	0.48783	0.534032	0.589098	0.657412	0.758575	0.860492
	ϵ	51.9282	42.808	39.8352	38.0814	36.9869	36.3888	36.4579
cerebro-spinal fluid	σ	2.284	2.3	2.31976	2.35177	2.40071	2.45981	2.53462
	ϵ	73.658	69.2142	68.9712	68.5265	68.3686	68.0985	67.7254
sclera, cornea	σ	0.937308	0.989455	1.03975	1.08974	1.65107	1.71981	1.80385
	ϵ	62.2115	56.58	54.5612	53.2269	52.2122	51.3822	54.0846
vitreous humour	σ	1.52	1.54	1.55976	1.60177	1.65107	1.71981	1.80385
	ϵ	68.8	68.4419	68.3024	68.2	67.9964	67.8755	67.6923
bladder	σ	0.2692	0.2692	0.2692	0.2692	0.2692	0.2692	0.2692
	ϵ	21.89	21.89	21.89	21.89	21.89	21.89	21.89
nerve	σ	0.404	0.462903	0.499756	0.533548	0.580714	0.634906	0.683077
	ϵ	44.36	37.8258	35.7122	34.3645	33.6893	33.1509	32.7846
cartilage	σ	0.524615	0.602903	0.649756	0.713548	0.791071	0.86984	0.953846
	ϵ	54.2388	45.9952	43.6544	42.1008	41.0179	40.2566	39.6538
gall bladder	σ	1.398	1.398	1.398	1.398	1.398	1.398	1.398
	ϵ	104.62	104.62	104.62	104.62	104.62	104.62	104.62
thyroid	σ	0.784	0.862903	0.0.909756	0.963548	1.03107	1.09981	0.1.17385
	ϵ	67.72	55.9806	52.9171	51.1468	50.0893	49.4264	48.9769
stomach	σ	0.554495	0.62367	0.673109	0.72619	0.790353	0.876092	0.973937
esophagus	ϵ	52.2269	45.3	42.9309	41.4103	40.3993	39.6647	39.0604
lung	σ	0.2734	0.2734	0.2734	0.2734	0.2734	0.2734	0.2734
	ϵ	38.39	38.39	38.39	38.39	38.39	38.39	38.39
kidney	σ	0.8893	0.8893	0.8893	0.8893	0.8893	0.8893	0.8893
	ϵ	117.43	117.43	117.43	117.43	117.43	117.43	117.43
testis	σ	0.4933	0.4933	0.4933	0.4933	0.4933	0.4933	0.4933
	ϵ	82.33	82.33	82.33	82.33	82.33	82.33	82.33
lens	σ	0.7742	0.7742	0.7742	0.7742	0.7742	0.7742	0.7742
	ϵ	112.74	112.74	112.74	112.74	112.74	112.74	112.74
small intestine	σ	1.739	1.739	1.739	1.739	1.739	1.739	1.739
	ϵ	128.09	128.09	128.09	128.09	128.09	128.09	128.09

σ : conductivity in Siemens; ϵ : relative permittivity

helix; and δ is the voxel edge size; j, ω, ϵ_o, and π having their conventional meaning.

The technique generates far fields that are accurate while the near fields may suffer from errors up to 10%. In this case, however, the magnetic fields were replaced by their equivalent electric fields due to limitations of the simulation tool used (REMCOM, Inc.). The equivalent electric fields (representing the magnetic field) were 90° out of phase with the electric field and were arranged so as to from a closed loop around the magnetic field they represent. The amplitude of the fields was obtained from trial simulations which were compared with simulations of the actual helix antenna modeled in detail on a fine mesh (made of cells with an edge size of 0.5 mm). As the dimensions of the antenna are much smaller than the operating wavelength, the helix modeled here operates in the normal mode. The monofilar helix antenna modeled had a diameter of 8 mm, length of 4 mm, and pitch of 1 mm (four turns). Its free-space vertical to horizontal polarization ratio (E_θ/E_ϕ) was 13 dB with an electric field left-circular polarization to right-circular polarization ratio of about 3.5 dB making the radiated field predominantly linear. Short simulations of the helix in free-space verified that the axial ratio was satisfied.

Three orientations of the source in the intestine were considered. The orientations used were limited by the nature of the grid (comprising of Yee cells). The three orientations are all mutually orthogonal. They are namely vertical, transverse and longitudinal and are shown in Fig. 1(c)–(e). Simulations were carried out for all three orientations at each source position considered. For all simulations, the body was suspended in free-space, hence, the effect of the presence of the ground is not

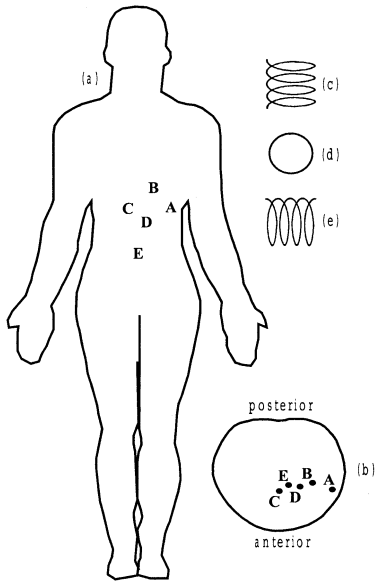

Fig. 1. Location and orientation of ingested sources. (a) Location in the vertical-transverse plane (subject facing toward the reader). (b) Location in the axial-transverse plane. (c) Vertical orientation. (d) Transverse orientation. (e) Longitudinal orientation.

taken into consideration. The effects of the ground will, however, have negligible effect on the fields in the proximity of the abdomen because the fields reaching the ground are so greatly attenuated.

The model of the helix does not take into account the effects of loading of the surrounding tissue that cause the impedance and, hence, the radiating efficiency of an antenna to change. Therefore, all the field results presented in this paper are normalized (using the overall maximum input power for the vertically oriented source at D) to the same radiation intensity, and reflect the effect of the body on the radiated fields excluding the associated effects on the radiating source.

Simulations were performed for sources at many locations in the GI tract. Three simulations, one for each orientation, were carried out at each location. In this paper, we present results for the five locations shown in Fig. 1, as an exhaustive presentation of all results is impractical in the space available. The selected results are representative of the overall results obtained. The locations were chosen such that the composition and morphology of the surrounding tissue at each position differed significantly from that of the others. The locations covered the whole extent of the small intestine and a range of depths into the body cavity in order to account for as many factors as possible that might influence the radiation of an ingested source. Simulations were run for a series of different frequencies in order to determine the influence of frequency and orientation on radiation. Fig. 1(a) and (b) shows five of the source positions considered in vertical-transverse and axial transverse cross sections, respectively. The positions are described in Table II.

TABLE II
DESCRIPTION OF POSITIONS

Position	Description
A	Near the skin, to the left.
B	Upper extent of the small intestine, behind the stomach.
C	Right extremity of the small intestine, next to the colon.
D	Central location. Most distant from any part of the colon of the five positions.
E	Lower extremity of the small intestine.

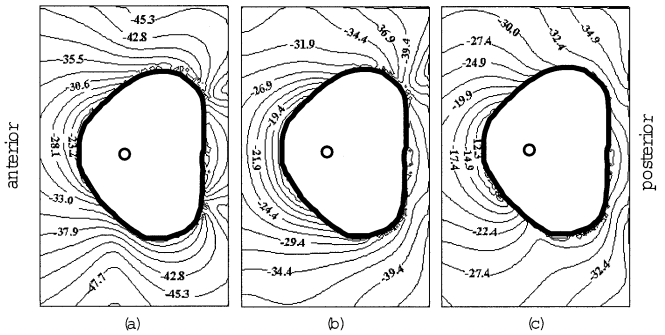

Fig. 2. Near fields in decibels for ingested 434-MHz source at E (circle denotes source position). (a) Vertically orientated. (b) Transversely orientated. (c) Longitudinally orientated.

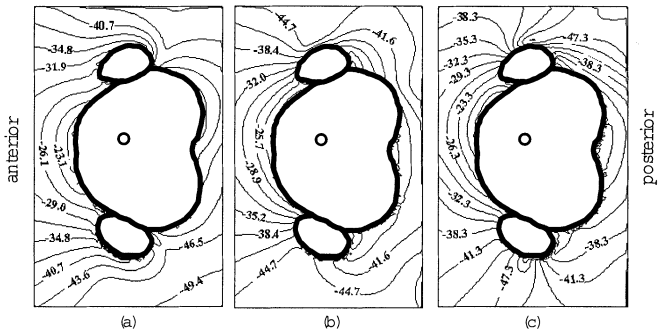

Fig. 3. Near fields in decibels for ingested 434-MHz source at D (circle denotes source position). (a) Vertically orientated. (b) Transversely orientated. (c) Longitudinally orientated.

III. RESULTS

A. Near Fields

A number of characteristics that generally apply to the radiation characteristics were identified. For deep-set centrally located (in the transverse plane) sources, we have symmetrical radiation for the vertical orientation, while longitudinally orientated sources give greater radiation in the transverse direction nearest to the outer surface (right or left) than vertically oriented sources. Transverse oriented sources radiate more in the posterior direction and at times in the anterior direction, compared with vertically oriented sources (see Figs. 2–4). For deep-set sources, longitudinally oriented sources give maximum radiation while vertically oriented sources give the least radiation as shown in Figs. 2 and 3. In contrast, as Fig. 4 illustrates, vertically oriented sources near the surface tend to give greater radiation than horizontally polarized sources. This seems to imply that the anatomy of the gut region in general offers greater hindrance to vertically polarized than to horizontally polarized fields. The change of radiation with change of orientation from vertical to

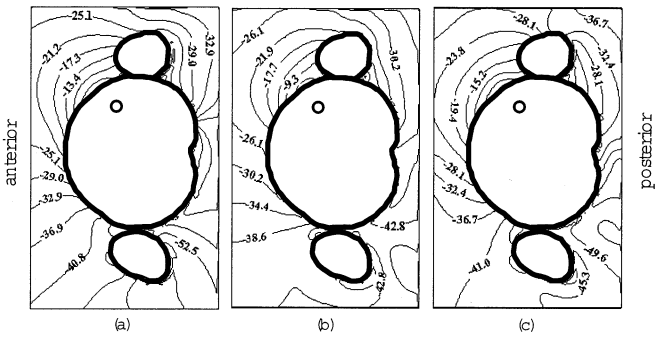

Fig. 4. Near fields in decibels for ingested 434-MHz source at A (circle denotes source position). (a) Vertically orientated. (b) Transversely orientated. (c) Longitudinally orientated.

horizontal was more significant for sources at E compared with sources at other locations. This characteristic was reflected in the far-field plots as well and the data infers that the anatomy surrounding E offers the greatest hindrance to vertically polarized fields. As would be expected, the more deep set the source is, the greater the radiation in the posterior direction.

The lowest radiated fields for all orientations were for sources positioned at D. The significant difference of the anatomy around this position compared with other locations is the relative distance from the colon to the direction of the maximum radiated fields.

The near-field intensities at different frequencies for a source positioned at E are shown in Fig. 5. The near-field intensity was found to first increase and then decrease with increasing frequency. This Gaussian-form relationship of the near radiated field intensity to frequency can be explained by taking into account the interaction of the reflected, scattered, and refracted fields within the gut. Reflection at boundaries is relatively small in most cases since the body tissues have similar properties. However, reflection is greatest at boundaries between fat and any other tissue and at the skin-air interface due to the large difference in permittivity at these boundaries. The result of the interaction of the incident, reflected, scattered, and refracted fields at lower frequencies is a net reduction in the fields within the gut and, consequently, the externally radiated field. This characteristic diminishes with increasing frequency resulting in higher internal and, thus, radiated field intensities. This accounts for the initial electric field intensity increase with frequency. The subsequent fall of field intensity with increasing frequency is due to the rapidly increasing absorption of electromagnetic fields by body tissue. Although the absorption of electromagnetic energy increases rapidly above 500 MHz due to the high losses caused by high water content body tissues [23], the reduction in the near radiated fields begins to take place at higher frequencies. These frequencies range from as low as 650 to as high as 900 MHz depending on the position of the radiating source. The radiated field intensity falls rapidly above 1 GHz.

Fig. 6 shows the near field in the absence of arms for a vertically orientated source at position D. The arms were removed since in the model that was used they were positioned such that they covered the front of the abdomen obstructing radiation directly in front and around positions D and E. The field remains fundamentally unchanged in the anterior direction. However, the field to the sides and the back increase considerably in the absence of arms, implying that the arms shield the sides and back from this radiation. This infers that there is a creeping wave on the body surface originating at the region of maximum radiation.

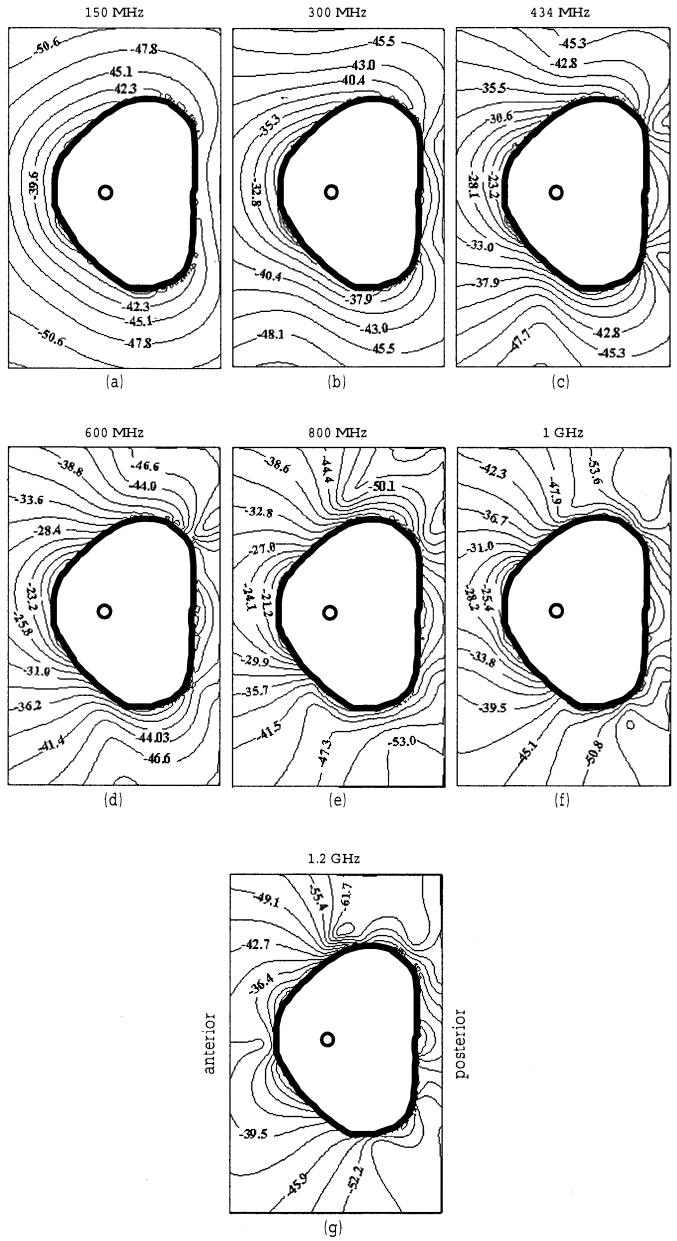

Fig. 5. Near fields in decibels for vertically orientated ingested source at E (circle denotes source position). (a) 150 MHz. (b) 300 MHz. (c) 434 MHz. (d) 600 MHz. (e) 800 MHz. (f) 1 GHz. (g) 1.2 GHz.

B. Far Fields

There are similarities in the patterns and magnitude of the vertically polarized (E_θ) far fields from vertically oriented sources. There are nulls in the E_θ patterns in the azimuth between 30° and 40° and, 140° and 170° in all cases except for the case of the source at E. For the source at E, the null is at about 90°. These nulls may be attributed to the two masses of retral muscles (mainly the Gluteus, Piriformis, Multifidus, Erector spinae, and Iliacus muscles) that run on either side of the spine. The ra-

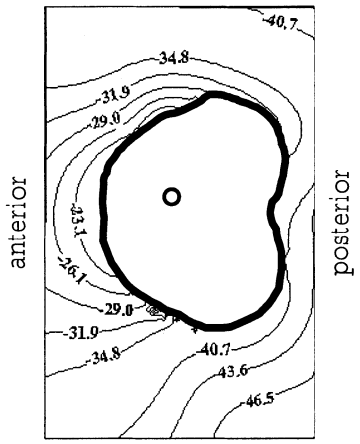

Fig. 6. Near fields in decibels for ingested 434-MHz vertically orientated source at D with no arms present (circle denotes source position).

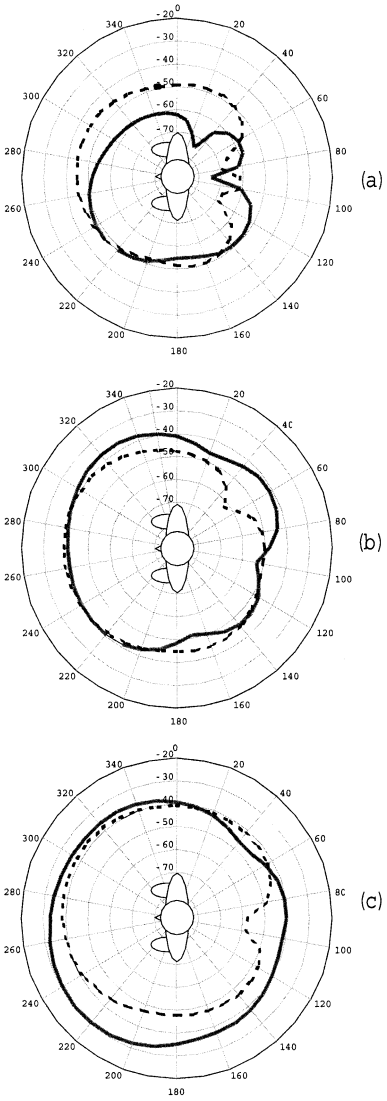

Fig. 7. Azimuthal far fields for ingested 434-MHz source at E. (a) Vertically orientated. (b) Transversely orientated. (c) Longitudinally orientated. (dashed line). Vertically polarized pattern. (solid line) Horizontally polarized pattern.

diation pattern for a vertical source at E is symmetrical about the anterior-posterior plane. Thus, as in the case of the near field, the

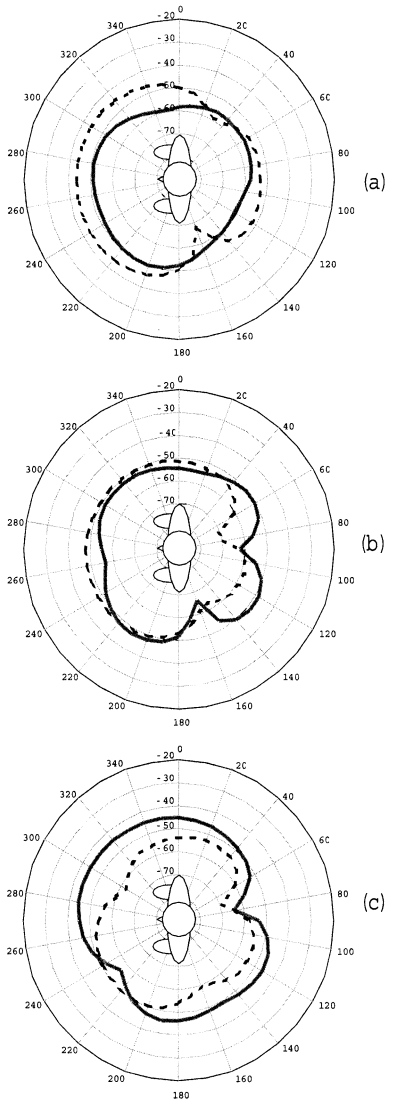

Fig. 8. Azimuthal far fields for ingested 434-MHz source at D. (a) Vertically orientated. (b) Transversely orientated. (c) Longitudinally orientated. (dashed line). Vertically polarized pattern. (solid line) Horizontally polarized pattern.

symmetrical far-field pattern is attributed to the anatomy in this region being relatively homogeneous. Radiation is most effective at the shortest distance from the source to the body surface in the azimuth direction as shown in Figs. 2–6. The fields that travel upwards and downwards within the body are so greatly attenuated that even after they are radiated they have little effect on the overall radiation pattern. There are three nulls in the radiation patterns of E_ϕ of vertically oriented sources at positions A and E at 30°, 90°, and about 160°, as is evident from Figs. 7(a), 8(a), and 9(a). Patterns for sources at B, C, and D all have one distinctive null, which falls within the 100°–150° range.

For transverse-oriented sources at A, D, and E, E_θ has a null between 70° and 100°. E_θ for sources at B and C, however, have nulls at 30° and 50°. For longitudinally oriented sources at E, the dominant polarization does not prevail and there is a strong, almost equal, amount of cross polarization, as shown in Fig. 7(b), inferring that in this case the radiation is due to predominant re-radiation that is vertically oriented to the body surface [11]. This effect does not, however, occur when the

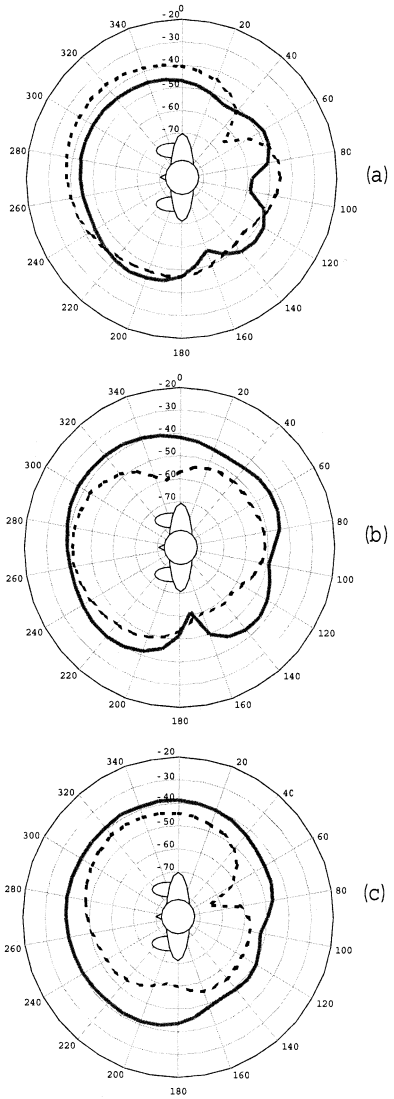

Fig. 9. Azimuthal far fields for ingested 434-MHz source at A. (a) Vertically orientated. (b) Transversely orientated. (c) Longitudinally orientated. (dashed line). Vertically polarized pattern. (solid line) Horizontally polarized pattern.

source is close to the body surface and, therefore, pertains only to sources set deep in the abdomen. These findings are consistent with the practical measured results in [11] probably because position E is close to the position of the vagina. The practical source used in [11] had a -15 dB cross polarization with respect to co-polar which compares well to the -13 dB cross polarization of the source model used here. However, this phenomenon only occurs when the source is at E. At other positions the cross polarization is not as strong and the same conclusion cannot be drawn. However, the result at E implies that the other results are also accurate. The relative difference in magnitude of the result presented here and that in [11] can be attributed to the difference between the practical antenna used in [11] and that of the antenna modeled here.

As in [11], there was generally a 10-dB difference between the anterior and posterior horizontal and vertical far fields. The maximum radiation is generally in the anterior direction (30°–150°). The 10-dB or more difference between the posterior and anterior far fields is attributed to the two masses of retral

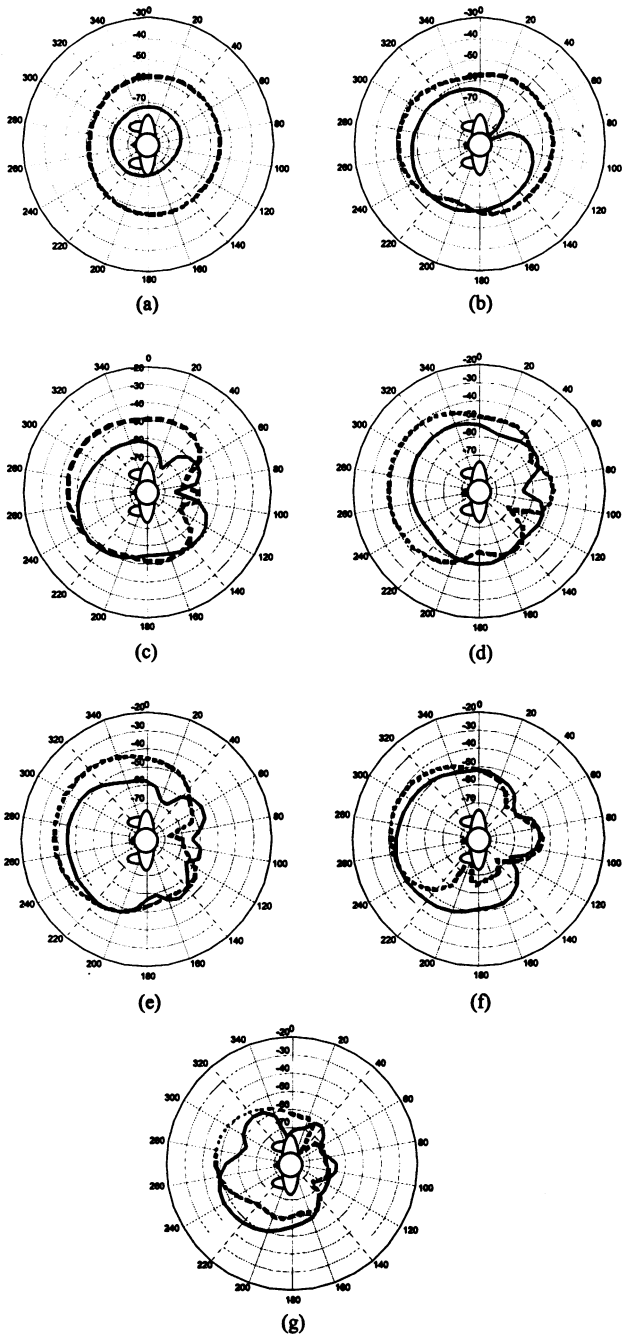

Fig. 10. Azimuthal far fields for vertically orientated ingested source at E. (a) 150 MHz. (b) 300 MHz. (c) 434 MHz. (d) 600 MHz. (e) 800 MHz. (f) 1 GHz. (g) 1.2 GHz. (dashed line). Vertically polarized pattern. (solid line) Horizontally polarized pattern.

located muscles running on either side of the spine. Muscle, blood, and skin are the greatest electromagnetic field absorbing tissues in the human body [23]. In the abdominal region, fat and ligaments of tendon dominate. These do not cause as much attenuation as the thick dorsal muscle mass that runs down the back of the body. However, the difference between the posterior and anterior far fields is not as large at lower frequencies as shown in Fig. 10. This is attributed to the low absorption characteristic of human tissues at low frequencies.

It is interesting to note that a high maximum near-field radiation (close or equal to maximum radiation intensity for the

entire body) does not translate to high radiation in the far field. For example, radiation from a longitudinal source at D has a lower maximum near-field intensity than that for the source at E but its far-field intensity is greater. This is attributed to the total amount of energy absorbed by the body at each respective position. The greater the energy absorbed the lower the radiation efficiency and the magnitude of the far field. Indeed, the radiation efficiency of the source at D is 0.54% while that at E is 0.15%.

Fig. 10 shows the far field at a number of frequencies for a source at E. It should be noted that the effective radiated power, in the absence of the body was the same at all frequencies. Both E_θ and E_ϕ have a Gaussian shaped relationship with frequency. The respective radiation gain first increases then decreases with increasing frequency, reaching a maximum in the 0.6- to 1.0-GHz range. The frequency at which the gain is a maximum is a function of position and orientation of the source. The axial ratio is generally unaffected by frequency. In all cases, the magnitude of the far field changes considerably between 300 and 400 MHz while they are similar between 0.8 and 1 GHz. Pattern fragmentation (i.e. formation of side-lobes) increased with increasing frequency. In all cases, the least circular polarization of the radiated field was observed at 600 MHz.

IV. Conclusion

We have carried out a detailed study of the radiated properties of ingested sources in the small intestine. It should, however, be noted that these results only serve as a guide as humans vary significantly in posture, morphology, size, and weight.

There is no direct co-relation between the near and far fields. This could be attributed to the phase variations of the near field perhaps contributing to nonintuitive far-field variations, and also to the presence of reactive fields in the near fields that do not contribute to the far field. However, both the near and far-field results show that maximum radiation is experienced on the anterior side of the body from radiation sources in the small intestine. The results suggest that implanted devices are most efficient in the 450 to 900 MHz range. The recommended pan-European frequency allocation for short range device applications and general telemetry applications falls at the lower and upper limits of this band, respectively. The US FCC regulations US209 and S5.150 also falls at the lower and upper limits of this band. The US FCC regulation US350 (608–614 MHz) is located almost in the middle of this band. The maximum far fields occur in the 600 MHz to 1 GHz range, which covers the recommended pan-European frequency of 900 MHz. There is some similarity in radiated patterns for several source orientations and locations. The radiated field intensity falls rapidly with frequencies above 1 GHz.

Though horizontally polarized sources cause strong cross polarization for sources at E this is not the case at other positions. For the majority of locations in the small intestine, vertically polarized radiation is more greatly attenuated than horizontal radiation. Clearly, the anatomy around the E region affects electromagnetic fields differently from the rest of the gut. There is a significant difference between the radiation characteristics of a source deeply set in the body and one close to the surface.

Specific absorption rate studies need to be carried out to determine the safety of these devices. However, since typical low range telemetry devices have powers of less than a few milliwatts ([25], [26], and [28]) it is unlikely that they will pose any RF hazard.

References

[1] N. C. Besseling, D. C. van Maaren, and Y. J. Kingma, "An implantable biotelemetry transmitter for six differential signals," *Med. Biol. Eng.*, pp. 660–664, Nov 1976.

[2] B. Hansen, K. Aabo, and J. Bojsen, "An implantable, externally powered radiotelemetric system for long-term ECG and heart-rate monitoring," *Biotelemetry Patient Monit.*, vol. 9, pp. 227–237, 1982.

[3] D. C. Jeutter and E. Fromm, "A modular expandable implantable temperature biotelemeter," *IEEE Trans. Biomed. Eng.*, vol. BME-27, pp. 242–247, 1980.

[4] W. H. Ko, J. Hynecek, and J. Homa, "Single frequency RF powered ECG telemetry system," *IEEE Trans. Biomed. Eng.*, vol. BME-26, pp. 105–109, Feb. 1979.

[5] J. D. Pauley and M. Reite, "A microminature hybrid multichannel implantable biotelemetry system," *Biotelemetry Patient Monit.*, vol. 8, pp. 163–172, 1981.

[6] B. C. Towe, "Passive biotelemetry by frequency keying," *IEEE Trans. Biomed. Eng.*, vol. BME33, pp. 905–909, Oct. 1986.

[7] *A Handbook on Biotelemetry and Radio Tracking*, C. J. Amlaner Jr. and D. W. MacDonald, Eds., Pergamon, New York, 1979, pp. 279–286.

[8] W. G. Scanlon and N. E. Evans, "RF performance of a 418-MHz radio telemeter packaged for human vaginal placement," *IEEE Trans. Biomed. Eng.*, vol. 44, pp. 427–430, May 1997.

[9] ——, "Numerical analysis of bodyworn UHF antenna systems," *Inst. Elect. Eng. Electron. Commun. Eng. J.*, vol. 13, pp. 53–64, Apr. 2001.

[10] G. Lazzi and O. P. Gandhi, "On modeling and personal dosimetry of cellular telephone helical antennas with FDTD code," *IEEE Trans. Antennas Propagat.*, vol. 46, pp. 525–530, Apr. 1998.

[11] W. G. Scanlon and N. E. Evans, "Radiowave propagation from a tissue-implanted source at 418 MHz and 916.5 MHz," *IEEE Trans. Biomed. Eng.*, vol. 47, pp. 527–534, Apr. 2000.

[12] J. Toftgard, S. N. Hornsleth, and J. Andersen, "Effects on portable antennas of the presence of a person," *IEEE Trans. Antennas Propagat.*, vol. 41, pp. 739–746, June 1993.

[13] M. A. Jensen and Y. Rahmat-Samii, "The electromagnetic interaction of handset antennas and a human in personal communications," in *IEEE Proc.*, vol. 83, Jan. 1995, pp. 7–17.

[14] M. Okoniewski and M. A. Stuchly, "A study of the handset antenna and human body interaction," *IEEE Trans. Microwave Theory Tech.*, pt. 2, vol. 44, pp. 1855–1864, Oct. 1996.

[15] J. S. Colburn and Y. Rahmat-Samii, "Human proximity effects on circular polarized handset antennas in personal satellite communications," *IEEE Trans. Antennas Propagat.*, vol. 46, pp. 813–820, June 1998.

[16] G. Iddan, G. Meron, A. Glukhovsky, and P. Swain, "Wireless capsule endoscopy," *Nature*, vol. 405, no. 6785, May, 25 2000.

[17] "Recommendation 70-03 relating to the use of short range devices (SRD)," in *Conf. Eur. Postal Telecomm. Admin. (CEPT)*, Tromso, Norway, 1997, CEPT/ERC/TR70-03.

[18] Z. P. Liao, H. L. Wong, B. P. Yang, and Y. F. Yuan, "A transmitting boundary for transient wave analysis," *Scientia Sinica*, ser. A, vol. 27, no. 10, pp. 1063–1076, Oct. 1984.

[19] J. P. Berenger, "PeRFectly matched layer for FDTD solution of wave-structure interaction problems," *IEEE Trans. Antennas Propagat.*, vol. 44, pp. 110–117, Jan. 1996.

[20] "Electronic Imaging: Board of Regents," National Institutes of Health National Library of Medicine (U.S.) Board of Regents, Bethesda, MD, Tech. Rep. NIH 90-2197, 1990.

[21] R. J. Luebbers and J. Beggs, "FDTD calculation of wide-band antenna gain and efficiency," *IEEE Trans. Antennas Propagat.*, vol. 40, no. 11, pp. 1403–1407, 1992.

[22] S. Wanatabe and M. Taki, "An improved FDTD model for the feeding gap of a thin-wire antenna," *IEEE Microwave Guide Wave Lett.*, vol. 8, no. 4, Apr. 1998.

[23] E. H. Grant, "The physical interaction of electromagnetic fields with people," in *Proc. Conf. Electromag. Fields Human Health*, 1991, pp. 1.2.1–1.2.5.

[24] A. Taflove, *Computational Eelectrodynamics: The Finite-Difference Time-Domain Method*. Norwood, MA: Artech, 1995.
[25] L. Wang *et al.*, "Integrated micro-instrumentation for dynamic monitoring of the gastro-intestinal tract," presented at the *2nd Annu. Int. IEEE-EMBS Special Topic Conf. Microtechnologies in Medicine and Biology*, Madison, WI, May 2–4, 2002.
[26] H. J. Park *et al.*, "Design of bi-directional and multi-channel miniaturized telemetry module for wireless endoscopy," presented at the *Proc. 2nd Annu. Int. IEEE-EMBS Special Topic Conf. Microtechnologies in Medicine and Biology*, May 2–4, 2002.
[27] M. Appleyard *et al.*, "A radomized trial comparing wireless capsule endoscopy with push enteroscopy for detection of small-bowel lesions," *Amer. Soc. Gastrointestinal Endoscopy—Gastrointestinal Endoscopy*, vol. 119, no. 6, pp. 1431–1438, 2000.
[28] F. Gong, P. Swain, and T. Mills, "Wireless endoscopy," *Amer. Soc. Gastrointestinal Endoscopy—Gastrointestinal Endoscopy*, vol. 51, no. 6, pp. 725–729, 2000.

Lawrence C. Chirwa received the B.Eng. degree in electronics and telecommunications from the University of Zambia, Lusaka, Zambia, in 1989, the M.Sc. degree in communications and real-time electronic systems from the University of Bradford, West Yorkshire, U.K., in 1991 and the PhD. degree from Hokkaido University, Sapporo, Japan, in 2000.

He was a lecturer with the Department of Electrical and Electronic Engineering, the University of Zambia from 1991 to 1996. He is a Researcher with University of Glasgow, Glasgow, U.K. His research interests include computational electromagnetics, finite-difference time-domain analysis, electromagnetic propagation, electromagnetic interaction with the human body, electromagnetic compatibility, and rapid waveguide time-domain analysis techniques.

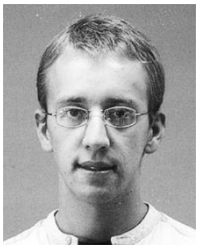

Paul A. Hammond (S'02) received the M.A. and M.Eng. degrees from the University of Cambridge, Cambridge, U.K. He is currently working towards the Ph.D. degree at the University of Glasgow, Glasgow, U.K., where he is developing CMOS sensor devices and circuits for ingestible diagnostics.

He has been an intern with STMicroelectronics, Bristol, U.K., working on analogue CMOS and board level design for test.

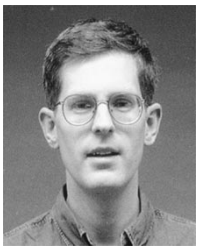

Scott Roy received the Ph.D. degree from the University of Glasgow, Glasgow, U.K. in 1994, for investigations into the engineering and architectural aspects of extended single electronic systems.

He is a Lecturer with the Department of Electronics and Electrical Engineering, University of Glasgow. His interests include high-performance computing and its application to device and systems modeling. He develops codes to simulate and optimize n-channel SiGe FETs for RF applications, and applies commercial codes to novel device and antenna systems.

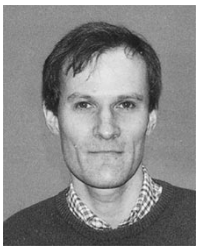

David R. S. Cumming (M'97) received the B.Eng. degree from Glasgow University, Glasgow, U.K., and the Ph.D. degree from Cambridge University, Cambridge, U.K., in 1989 and 1993, respectively.

He has worked variously on mesoscopic device physics, RF characterization of novel devices, fabrication of diffractive optics for optical and submillimeter wave applications, and microelectronic design. He is a Senior Lecturer and EPSRC Advanced Research Fellow in Electronics and Electrical Engineering at the University of Glasgow, Glasgow, U.K., where he leads the Microsystem Technology Group.